

Novel Lithium-Sulfur Polymer Battery Operating at Moderate Temperature

Vittorio Marangon,^[a] Daniele Di Lecce,^[b] Luca Minnetti,^[b] and Jusef Hassoun^{*,[a, b, c]}

A safe lithium-sulfur (Li-S) battery employs a composite polymer electrolyte based on a poly(ethylene glycol) dimethyl ether (PEGDME) solid at room temperature. The electrolyte membrane enables a stable and reversible Li-S electrochemical process already at 50 °C, with low resistance at the electrode/electrolyte interphase and fast Li⁺ transport. The relatively low molecular weight of the PEGDME and the optimal membrane composition in terms of salts and ceramic allow a *liquid-like* Li-S conversion reaction by heating at moderately high temperature, still holding the *solid-like* polymer state of the cell. Therefore, the electrochemical reaction of the polymer Li-S cell is characterized by the typical dissolution of lithium polysulfides

into the electrolyte medium during discharge and the subsequent deposition of sulfur at the electrode/electrolyte interphase during charge. On the other hand, the remarkable thermal stability of the composite polymer electrolyte (up to 300 °C) suggests a lithium-metal battery with safety content significantly higher than that using the common, flammable liquid solutions. Hence, the Li-S polymer battery delivers at 50 °C and 2 V a stable capacity approaching 700 mAh g_S⁻¹, with a steady-state coulombic efficiency of 98%. These results suggest a novel, alternative approach to achieve safe, high-energy batteries with solid polymer configuration.

1. Introduction


The lithium-sulfur (Li-S) cell is one of the most promising next-generation battery systems, benefiting from the multi-electron conversion process $S_8 + 16Li^+ + 16e^- \rightleftharpoons 8Li_2S$,^[1,2] which leads to a theoretical energy density as high as 2600 Wh kg⁻¹, when referred to the Li₂S mass.^[3] This reaction occurs via formation of several lithium polysulfides (Li₂S_x, 2 ≤ x ≤ 8)^[4,5] which are soluble in the electrolyte solution for x ≥ 4 and may migrate to the lithium anode, causing active material loss and cell degradation by reaction at the electrode surface.^[6] Significant effort has been devoted over the past decade to optimize suitable cathode architectures that may mitigate the low electronic


conductivity of S, Li₂S₂, and Li₂S and provide suitable reaction sites for the lithium polysulfides.^[7] So far, a large variety of electrode compositions involving various additives, such as carbon matrices,^[8-12] MOFs,^[13-15] and metal nanoparticles,^[16,17] have been proposed. On the other hand, the addition of sacrificial agents to the electrolyte solution, e.g., LiNO₃,^[18,19] has proven to be the key strategy to actually mitigate the detrimental effects of polysulfide dissolution via formation of a stable solid electrolyte interphase (SEI) on the lithium anode.^[20] Furthermore, electrolyte additives may inhibit metallic-dendrite growth, that is, an undesired process hindering the large-scale application of rechargeable lithium-metal batteries.^[20,21] Significant improvements have been achieved by developing alternative electrolyte formulations to those employed in conventional lithium-ion batteries, which react with the lithium polysulfides.^[22] In this regard, liquid solutions of lithium salts with large anions and LiNO₃ in 1,3-dioxolane:1,2-dimethoxyethane (DOL:DME) mixtures are chemically stable towards lithium polysulfides, form a suitable film over the anode, have a low viscosity and high ion conductivity, thereby enabling high performance of the Li-S cell.^[23] However, excessive volatility and high flammability of these interesting electrolyte media pose safety concerns, in particular in cells using lithium metal.^[10] Alternative electrolyte systems employing liquid end-capped glymes as solvents, such as poly(ethylene glycol) dimethyl ether (PEGDME, CH₃O(CH₂CH₂O)_nCH₃) with a low n value,^[24-26] have a reasonably high flash point.^[27] On the other hand, long-ether-chain PEGDME with average molecular weight (MW) higher than 1000 g mol⁻¹ (moderately high n value) is a solid with semi-crystalline structure, low flammability, and negligible volatility at room temperature. Solid polymer electrolytes using poly(ethylene-oxide) (PEO) have remarkable thermal, mechanical, and electrochemical stability, along with high compatibility with various lithium salts and enhanced Li⁺ ions transport.^[28]

[a] V. Marangon, Prof. J. Hassoun
Department of Chemical,
Pharmaceutical and Agricultural Sciences
University of Ferrara
Via Fossato di Mortara 17,
Ferrara, 44121, Italy
E-mail: jusef.hassoun@unife.it

[b] Dr. D. Di Lecce, L. Minnetti, Prof. J. Hassoun
Graphene Labs
Istituto Italiano di Tecnologia
via Morego 30, Genova,
16163, Italy
E-mail: jusef.hassoun@iit.it

[c] Prof. J. Hassoun
National Interuniversity Consortium of Materials Science
and Technology (INSTM)
University of Ferrara Research Unit
Via Fossato di Mortara, 17, 44121,
Ferrara, Italy

 Supporting information for this article is available on the WWW under <https://doi.org/10.1002/celec.202101272>

 © 2021 The Authors. ChemElectroChem published by Wiley-VCH GmbH. This is an open access article under the terms of the Creative Commons Attribution License, which permits use, distribution and reproduction in any medium, provided the original work is properly cited.

However, excessive crystallinity at room temperature due to the relatively high molecular weight (that is, typically higher than $100000 \text{ g mol}^{-1}$) limited the large-scale application PEO-based polymer electrolytes, to date commercialized in niche automotive and stationary-storage sectors that allow a higher operating temperature.^[21] Indeed, suitable ionic conductivity ($> 10^{-4} \text{ S cm}^{-1}$) and adequate Li^+ transport properties are typically achieved at the predominantly amorphous state of the PEO above 65°C ,^[29] which allows battery application employing insertion^[30–33] or sulfur-based conversion cathodes.^[34–39] The use of ceramic fillers such as SiO_2 , Al_2O_3 , TiO_2 or ZrO_2 generally promotes the amorphous phase in PEO and enhances the ionic conductivity, although the polymer cannot be applied below 60°C .^[29,40,41] In this regard, solid PEGDME has mechanical and chemical stability compatible with lithium cell application, and a melting point allowing operation at lower temperature compared to PEO.^[42] Indeed, in our earlier report a $\text{Li}|\text{LiFePO}_4$ battery exploited a solid PEGDME-based composite polymer electrolyte (PEGDME_CPE) incorporating SiO_2 ceramic, lithium bis(trifluoromethanesulfonyl)imide (LiTFSI) as conductive salt, and LiNO_3 as SEI-forming agent.^[42] The above cell operated at 50°C and delivered reversibly 125 mAh g^{-1} , with a capacity retention as high as 99% over 300 cycles.^[42] This electrolyte formulation benefitted from advantageous electrochemical and thermal properties that set between those of the well-known solid PEO-based electrolytes (PEO_PEs)^[41] used in the typical Li-polymer cell, and the common DOL:DME-based liquid electrolytes (DOL:DME_LEs) employed in the Li–S battery.^[23] Notably, the former electrolytes may significantly enhance the safety content of the cell with respect to the latter, although they typically suffer from poor Li^+ transport properties at moderate

temperatures.^[41] Therefore, we explore in this work the applicability of the PEGDME_CPE in high energy Li–S batteries working at moderate temperature (i.e., 50°C). It is worth mentioning that a Li–S cell exploiting a solid polymer electrolyte synthesized by using a liquid PEGDME with average MW of 250 g mol^{-1} as the starting precursor was previously achieved.^[43] On the other hand, the Li–S cell reported herein originally employs a pristine PEGDME with average MW of 2000 g mol^{-1} (PEGDME2000) as solid polymer matrix to achieve the composite membrane.^[44] We investigate the ion transport, the thermal properties and the electrode/electrolyte interphase, and demonstrate the efficient operation at 50°C of the lithium-sulfur polymer battery which is allowed by the relatively low molecular weight of the selected PEGDME.

2. Results and Discussion

To better evaluate the differences between the various electrolyte configurations, Figure 1 reports a comparison between solid PEO_PEs^[41] and PEGDME_CPE, and a DOL:DME_LE solution in terms of Li^+ transference number (t^+) measured at the optimal operative temperature of each medium (Figure 1a) and ionic conductivity at 50°C (Figure 1b). In this work, the “optimal operative temperature” refers to the most adequate temperature value for allowing efficient operation in a Li–S cell depending on the employed solvent, that is, 25°C for DOL:DME solutions,^[23,45–47] 50°C for the PEGDME2000,^[42] and 80°C for PEO.^[41] The DOL:DME_LE exhibits a significantly higher t^+ at room temperature compared to that of PEGDME_CPE at 50°C , that is, 0.67 vs. 0.23 (Figure 1a, and Figure S1a and Table S1 in

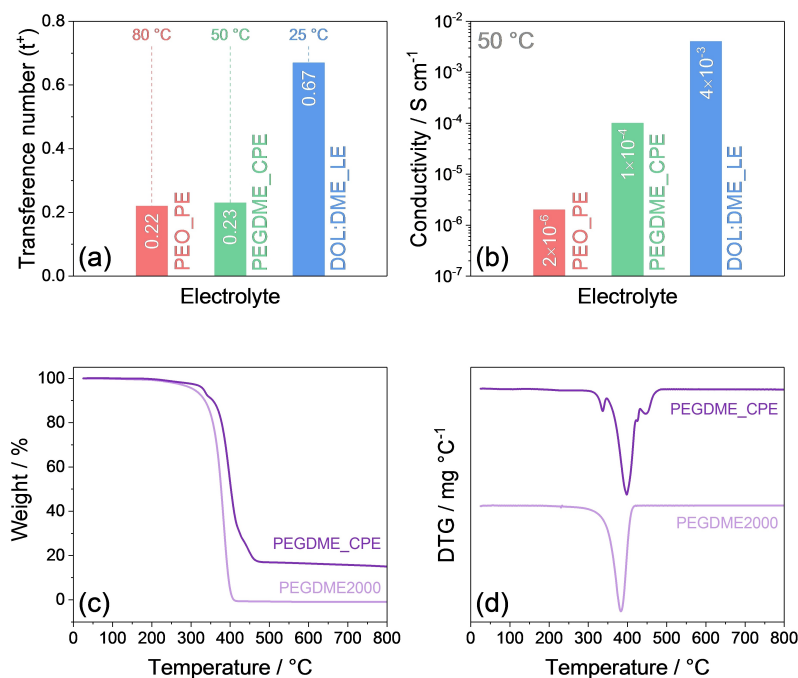


Figure 1. (a) Lithium transference number (t^+) at the selected operating temperature and (b) ionic conductivity at 50°C of solid PEO_PEs,^[41] PEGDME_CPE, and DOL:DME_LE (see Experimental section for details on sample composition); (c) TGA and (d) DTG curves of the PEGDME_CPE and the PEGDME2000 powder recorded under N_2 in a temperature range between 25°C and 800°C at a heating rate of 5°C min^{-1} . See the Experimental section for sample acronyms.

Supporting Information),^[42] while the PEO_PE has a t^+ of 0.22 at 80 °C.^[41] Relevantly, the PEGDME_CPE has ionic conductivity exceeding by two order of magnitude that of PEO_PE at 50 °C (1×10^{-4} with respect to $2 \times 10^{-6} \text{ S cm}^{-1}$ in Figure 1b).^[41,42] Despite being adequate for battery application, the conductivity of PEGDME_CPE at the latter temperature is 10 times lower than that of the DOL:DME_LE at 25 °C due to the higher mobility of the ions in the solution compared to the solid polymer (see Figure S1b in Supporting Information for further details on these measurements).^[42] These data suggest that the PEGDME_CPE might enable satisfactory ion motion at moderate temperature, which is considered a key requirement for application in lithium-sulfur polymer cells,^[21] although possible issues in the experimental determination of t^+ leading to an overestimation of the calculated value cannot be completely excluded.^[48,49] We remark that the relatively low molecular weight of the PEGDME used for achieving the polymer electrolyte (average MW = 2000 g mol^{-1} , see the Experimental section for further details) may actually allow suitable battery performance, superior safety level, and a lithium-sulfur conversion process below the conventional application temperature of PEO-based electrolytes.^[50] Indeed, PEO_PE requires a higher temperature than PEGDME_CPE to reach a comparable t^+ (i.e., 80 °C rather than 50 °C in Figure 1a) due to the relevantly higher molecular weight (i.e., 600000 g mol^{-1} vs 2000 g mol^{-1}). Furthermore, Figure S2 in the Supporting Information also demonstrates the applicability of the PEGDME_CPE at higher temperatures, as the electrolyte exhibits an ionic conductivity of $4 \times 10^{-4} \text{ S cm}^{-1}$ at 80 °C. In this regard, the PEGDME_CPE shows high thermal stability, as confirmed by thermogravimetric analysis (TGA) under inert atmosphere of Figure 1c (see Figure 1d showing the corresponding differential thermogravimetry, i.e., DTG). The thermal analysis of the solid PEGDME2000 polymer, reported in the same figure for comparison, reveals a single weight loss starting at about 280 °C and centered slightly above 380 °C, which suggests a large application temperature range. On the other hand, the PEGDME_CPE exhibits three weight-loss steps: the first one is centered at 340 °C and might be ascribed to removal of the fraction of PEGDME2000 chains that interact with the SiO_2 particles,^[51] the second one occurs at 400 °C and is likely related to complexes formed between PEGDME2000 and the lithium salts, which are characterized by higher decomposition temperature,^[52] the third one is observed in the temperature range from 420 °C to 470 °C and is mainly attributed to the decomposition of LiTFSI.^[53] Notably, 15 wt.% sample residues after the measurement mostly consist of SiO_2 along with chemical compounds formed by the decomposition of the lithium salts (LiTFSI and LiNO_3).^[53] Therefore, our composite polymer electrolyte ensures a high ionic conductivity, a suitable cation transference number for application in batteries exploiting the lithium metal anode, and a remarkable thermal stability (up to 280 °C).

The electrochemical response of the Li-S polymer battery employing the PEGDME_CPE is herein investigated by cyclic voltammetry (CV) and electrochemical impedance spectroscopy (EIS) from 50 to 80 °C, to demonstrate the actual applicability and stability of this cell configuration in a wide temperature

range. Figure 2 (a, c and e) reports the voltammograms of the cell tested consecutively at 50, 60 and 70 °C, respectively, whilst Figure S3a in Supporting Information shows that measured at 80 °C. Figure 2a reveals for the polymer battery a discharge process at 50 °C with current peaks at 1.94 and 2.33 V vs. Li^+/Li upon the first cycle, which are reflected as two charge signals at 2.28 and 2.60 V vs. Li^+/Li . This response is in part consistent with that of conventional Li-S batteries using liquid electrolyte solutions (Figure S4a in the Supporting Information), typically characterized by two discharge peaks at about 2.3 and 2.0 V vs. Li^+/Li , reflecting the reversible conversion of lithium and sulfur to soluble lithium polysulfides with various chain lengths (Li_2S_x with $4 \leq x \leq 8$) along with solid Li_2S_2 and Li_2S , and two overlapped charge signals around 2.3 V vs. Li^+/Li .^[54] The subsequent CV profiles of the polymer battery at 50 °C (Figure 2a) exhibit a shift of the discharge peaks to higher potentials likely due to improved reaction kinetics, and a raise of the charge peak at 2.28 V vs. Li^+/Li suggesting an enhancement of the polysulfide oxidation rate. According to earlier reports on Li-S cells using liquid electrolyte solutions,^[16,17,55,56] this activation upon cycling can be associated with micro-structural rearrangements in cathode which increase the sulfur utilization and enhance the electrode/electrolyte interphase. Further improvements in electrochemical activity can be achieved by rising the operating temperature, as shown in Figure 2c and 2e, as well as in Figure S3a of the Supporting Information. Indeed, an increase in temperature up to 60 (Figure 2c), 70 (Figure 2e) and 80 °C (Figure S3a) leads to a higher peak current upon charge and to a better overlap of the CV profiles (in particular at 60 and 70 °C), thus suggesting a very stable and reversible electrochemical process. Furthermore, a discharge peak appears slightly above 2 V vs. Li^+/Li when the temperature ranges from 60 to 80 °C, thereby indicating that the segmental motion of the polymer chains may assist the ionic transport through the electrolyte and at the electrode/electrolyte interphase during the conversion process.^[21] Furthermore, the presence of an additional reduction peak between 2.0 and 2.1 V vs. Li^+/Li observed in the CV measurements performed at 60, 70 and 80 °C, whose profiles are reported in Figures 2c, 2e and S3a, respectively, as well as the absence of a zero-current response at the end of cathodic scan, is likely ascribed to relatively slow kinetics for the formation of the various polysulfides in the PEGDME_CPE matrix, and actually indicates a partially reversible reaction. On the other hand, the reduction of S_8 to polysulfides in the lithium cell occurs through various reaction steps and leads to Li_2S_x species with different chain length within the full range of the discharge potential. These steps may be partially detected by voltammetry depending on the operating temperature, as indeed shown in Figure 2. In particular, the additional peaks at the lower potential during reduction may be reasonably ascribed to the kinetically hindered formation of low-chain polysulfides (such as Li_2S_4 and Li_2S_2). Notably, the significant polarization of the polymer cell upon charging at 50 °C leads to two distinct charge peaks in the CV (Figure 2a), while that employing the DOL:DME_LE (Figure S4a in the Supporting Information) displays broad, convoluted peaks during oxidation, which is in full agreement with

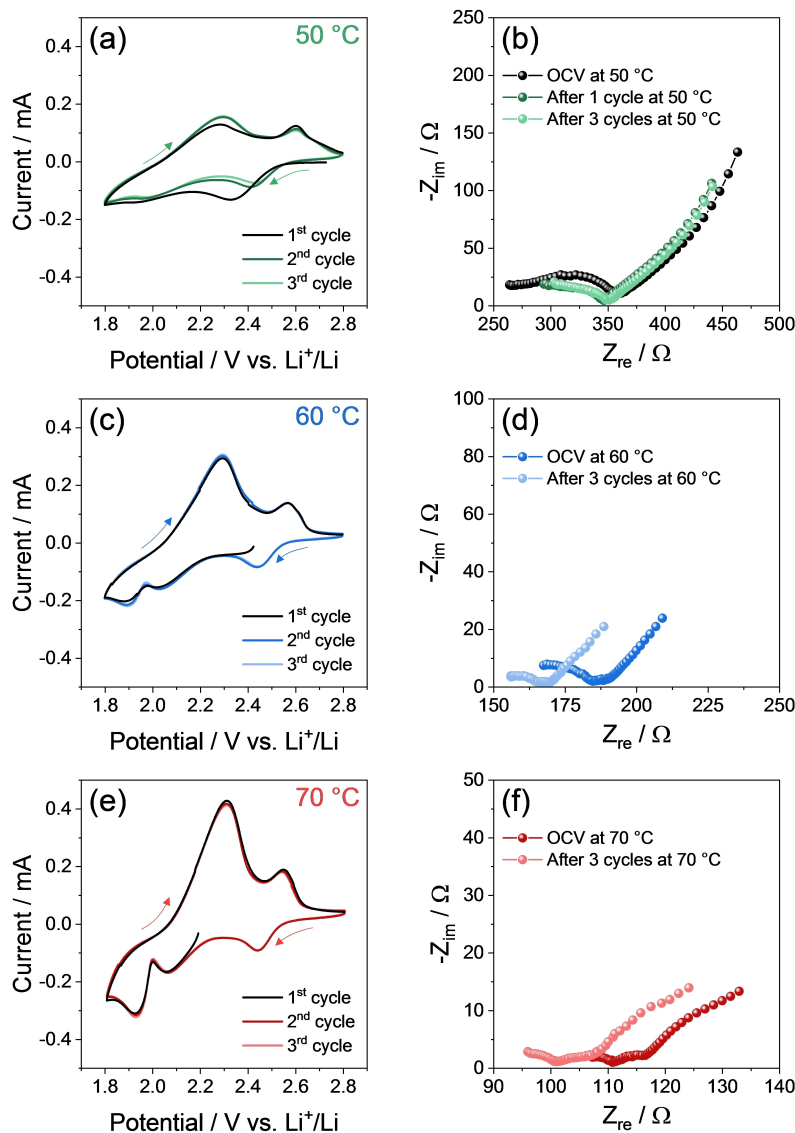


Figure 2. (a, c, e) CV curves and (b, d, f) EIS Nyquist plots of the Li|PEGDME_CPE|S:SPC 70:30 w/w cell at various temperatures, that is, (a, b) 50 °C, (c, d) 60 °C and (e, f) 70 °C. CV performed between 1.8 and 2.8 V vs. Li⁺/Li at 0.1 mV s⁻¹; EIS carried out at the open circuit voltage (OCV) condition of the cell as well as upon the voltammetry cycles, by applying an alternate voltage signal of 10 mV within the 500 kHz–100 mHz frequency range. See the Experimental section for sample acronyms and Table 1 for relevant parameters extracted by analysis of the EIS data.

the literature.^[57] Therefore, the different electrochemical response of the Li–S polymer cell compared to the Li–S conventional one using a liquid solution may be in part ascribed to the mobility of Li⁺ ions within the electrolyte medium and at the interphase between electrolyte and sulfur electrode. Accordingly, the polymer battery exhibits an electrochemical response approaching the *liquid-like* behavior as the temperature is gradually increased up to 80 °C. In this regard, further insight is given by Figure S5 and Table S4 in Supporting Information, which show that the above discussed charge voltammetry peaks shift toward each other at elevated temperature, whilst the discharge peaks attributed to the short polysulfides shift at higher potential. In particular, the 1st charge peak moves from 2.29 V vs. Li⁺/Li at 50 °C to 2.35 V vs. Li⁺/Li at 80 °C (Figure S5b), while the 2nd charge signal from 2.60 to 2.52 V vs. Li⁺/Li (Figure S5c), thereby leading to a gradual merging of these

peaks promoted by the increase in PEGDME chains mobility and Li⁺ ions conductivity.^[42] We remark that the polymer cell at 80 °C exhibits in CV a *liquid-like* performance (Figure S3a) similar to that of Li–S batteries employing low-molecular-weight glymes, typically characterized by a higher viscosity than that of conventional DOL:DME mixtures.^[58] Remarkably, the tests reported in Figure 2a, 2c, 2e, and in Figure S3a (Supporting Information) refer to 12 consecutive CV runs at various temperatures, thus suggesting a notable stability of the electrochemical process.

EIS measurements performed upon CV (see the Nyquist plots in Figure 2b, 2d, 2f, and Figure S3b the Supporting Information) reveal modifications at the electrode/electrolyte interphase in the Li–S polymer cell during cycling. Table 1 reports the results of non-linear least squares (NLLS) analyses of the corresponding spectra, in terms of equivalent circuits (i.e.,

Table 1. PEGDME_CPE bulk resistance (R_e) and S:SPC 70:30 w/w/PEGDME_CPE interphase resistances (R_1 , R_2) obtained by nonlinear least squares (NLLS) analysis of the EIS data via the Boukamp software.^[66,67] The EIS data have been collected at various temperatures during CV measurements on the Li|PEGDME_CPE|S:SPC 70:30 w/w cell. See the Experimental section for sample acronyms and Figure 2 for relevant voltammetry profiles and Nyquist plots.

Temperature [°C]	Cell condition	Circuit	R_e [Ω]	R_1 [Ω]	R_2 [Ω]	$R_1 + R_2$ [Ω]	χ^2
50 °C	OCV	$R_e(R_1Q_1)Q_w$	272 ± 1	83 ± 2	/	83 ± 2	5×10^{-6}
	1 CV cycle	$R_e(R_1Q_1)Q_w$	298 ± 2	44 ± 2	/	44 ± 2	4×10^{-6}
	3 CV cycles	$R_e(R_1Q_1)Q_w$	304 ± 3	42 ± 3	/	42 ± 3	3×10^{-6}
60 °C	OCV	$R_e(R_1Q_1)(R_2Q_2)Q_w$	150 ± 2	36 ± 2	3.4 ± 0.5	39 ± 2	2×10^{-6}
	3 CV cycles	$R_e(R_1Q_1)(R_2Q_2)Q_w$	151 ± 2	15 ± 3	2.3 ± 0.9	17 ± 3	1×10^{-5}
70 °C	OCV	$R_e(R_1Q_1)(R_2Q_2)Q_w$	102 ± 1	9 ± 1	3.9 ± 0.4	13 ± 1	8×10^{-7}
	3 CV cycles	$R_e(R_1Q_1)(R_2Q_2)Q_w$	90 ± 4	11 ± 4	3 ± 1	14 ± 4	9×10^{-6}

$R_e(R_1Q_1)Q_w$, see Experimental section), resistance values (i.e., R_e and R_i), and χ^2 parameter. The overall electrode/electrolyte interphase resistance ($R_1 + R_2$) of the polymer cell at 50 °C is represented by the width of the high-middle frequency semi-circles of the Nyquist plot (Figure 2b), and incorporates contributions by SEI film, electrode charge transfer, and possible grain boundaries.^[59] The above resistance drops from 83 Ω at the open circuit voltage (OCV) condition to stable values around 42 Ω after 3 voltammetry cycles (Table 1). This behavior indicates the occurrence of activation processes and consequent enhancement of the electrode/electrolyte interphase by favorable microstructural modifications upon cycling.^[16,17,55,56] The rise in operative temperature leads to a further decrease in the overall electrode/electrolyte resistance, thus reflecting the above-described improvements in conversion kinetics^[42] (see Figure 2d, 2f and Figure S3b in the Supporting Information), with final values of 17, 14 and 12 Ω at 60, 70, and 80 °C (see Tables 1 and S2 in the Supporting Information). In this regard, the resistance trends at various temperatures reported in Figure S6 in Supporting Information show that the charge transport through both the interphase and the electrolyte (panels a and b, respectively) are thermally activated processes. Indeed, the electrolyte interphase resistance measured after subsequent voltammetry cycles decreases from 304 Ω at 50 °C to 150 Ω at 60 °C, 90 Ω at 70 °C, and 55 Ω at 80 °C. The thermal activation of the charge transfer process is also observed by the increase of the (R_iQ_i) elements number in the equivalent circuit (Table 1 and Table S2 in the Supporting Information). Indeed, the difference between the circuits at 50 °C (Figure 2b) and at higher temperatures (Figure 2d, 2f, and Figure S3b in Supporting Information) reflects the modifications of the electrode/electrolyte interphase achieved through temperature rise, which cause the deconvolution of the high-middle frequency semi-circle into various contributors (SEI film, electrode charge transfer, and possible grain boundaries) represented by additional (R_iQ_i) elements. Relevantly, these changes are in line with the modification of the CV characteristics of the corresponding Li–S cell (Figure 2a, 2c, 2e and Figure S3a in Supporting Information). In addition, both the benchmark Li–S cell at room temperature using DOL:DME_LE and the polymer Li–S cell at 80 °C using PEGDME_CPE exhibit comparably low electrode/electrolyte interphase resistance, i.e., 2 Ω for the former and 12 Ω for the latter, which confirms that the polymer battery approaches the *liquid-like* condition. However, the ion motion is likely much

faster in the benchmark electrolyte which shows related resistance of about 5 Ω, with respect to the polymer one which has a resistance of 55 Ω after 3 CV cycles (see Tables S2 and S3 in the Supporting Information). It is worth mentioning that the contribution of the lithium anode in the EIS measurements is not negligible. Indeed, the discussions of Figures 2, S3 and S4 in the Supporting Information refer to an electrode/electrolyte interphase including both the cathode and the lithium side, whilst the study of the interphase formed between lithium and the PEGDME_CPE was already deeply considered in our late work,^[42] where EIS and lithium stripping/deposition tests performed on symmetrical Li|PEGDME_CPE|Li cells at 50 °C revealed a stable electrode/electrolyte interphase with low resistance and overvoltage. The affinity between lithium metal and the PEGDME_CPE is well confirmed by the EIS measurements reported in Figure 2 in which all the Li–S cells exhibit low overall resistance values and stable kinetics. Therefore, both the CV and the EIS data reveal that the electrochemical activity of the Li–S polymer battery is adequate at 50 °C, and enhanced by thermal activation within the wide operative temperature range extending from 50 to 80 °C.

Figure 3 illustrates the characteristics of the electrode/polymer electrolyte assembly by showing photographic images of a sample before and after cycling (panel a and b), along with TGA data (panel c and d), respectively, and SEM images (panel e; see the Experimental section for details on sample preparation). A direct comparison between the PEGDME_CPE hosted on the positive electrode in the pristine condition and after consecutive CV cycles performed at 50, 60, 70, and 80 °C reveals a change in color of the polymer membrane from white (Figure 3a) to a dark red (Figure 3b), which demonstrates the expected dissolution of the lithium polysulfides into the electrolyte upon the electrochemical process.^[60] It is worth mentioning that the dissolution of lithium polysulfides into the electrolyte, which is common process and not fully avoidable, does not necessarily lead to a compromising shuttle effect. In fact, the shuttle process that usually leads to an unlimited anodic reaction without charge accumulation and efficiency decrease is not observed in our tests, as indeed expected by the inclusion of the LiNO₃ additive into the PEGDME_CPE formulation, which promotes the formation of a protective SEI layer on the lithium surface.^[25] Relevantly, literature work reported a high performance semi-liquid Li–S battery exploiting lithium polysulfides directly dissolved into the electrolyte without any shuttle

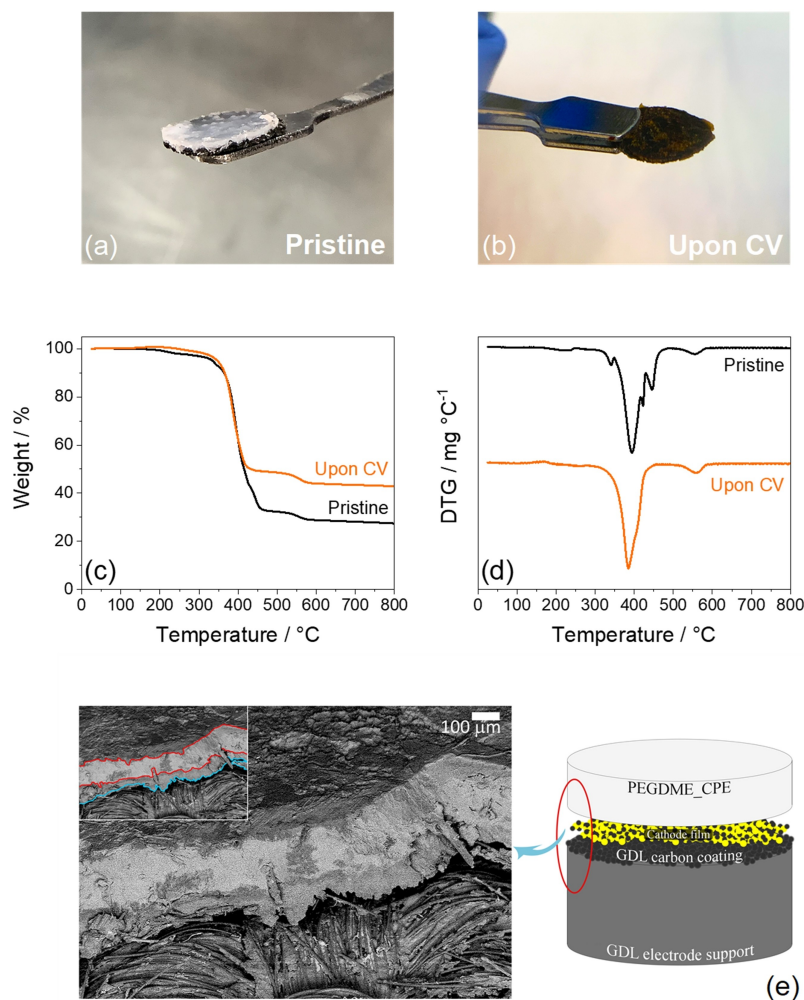


Figure 3. (a, b) Photographic images and (c) TGA curves with (d) corresponding DTG profiles of a PEGDME_CPE membrane on a S:SPC 70:30 w/w electrode (i.e., the PEGDME_CPE|S:SPC 70:30 w/w electrode assembly) (a) in the pristine condition (before assembling the cell) and (b) after CV in lithium cell at various temperatures (see Figure 2); TGA carried out under N_2 in the 25–800 °C temperature range by employing a heating rate of 5 °C min^{-1} . (e) SEM image (left-hand side) showing the PEGDME_CPE|S:SPC 70:30 w/w electrode assembly after CV in lithium cell at various temperatures (see Figure 2), with related graphic scheme (right-hand side); SEM inset highlights the presence of the assembly layers, i.e., (i) the PEGDME_CPE membrane (between red lines) and (ii) the carbon-sulfur electrode film (between bottom-red line and cyan line).

reaction, due to the above-mentioned protection of the lithium surface by $LiNO_3$ additive.^[58] TGA of the pristine and cycled PEGDME_CPE/electrode samples (Figure 3c, and 3d for corresponding DTG) indicates various weight losses, which are attributed to the components of the assembly. Thus, the pristine sample (black curves in Figure 3c and 3d) shows a weight loss between 230 and 300 °C due to sulfur evaporation from the positive electrode,^[61,62] along with two subsequent processes at 340 and 400 °C ascribed to the PEGDME2000, which are in agreement with the TGA of Figure 1. Furthermore, weight variations ascribable to LiTFSI are observed between 420 and 445 °C,^[53] and partial degradation of the electrode support likely occurs at about 560 °C. A residue of 27% of the initial weight after the heating scan accounts for $LiNO_3$,^[53] SiO_2 particles, and electrode support. The cycled sample exhibits rather different thermal behavior (orange curves in Figure 3c

and 3d) characterized by an increase in weight at about 130 °C, which likely reflects reactions between N_2 and the lithium polysulfides during the thermogravimetric experiment, followed by a slight decrease due to sulfur evaporation up to 300 °C.^[61,62] In addition, the loss of PEGDME2000 and LiTFSI appears as a single process centered at 390 °C, rather than the multiple losses between 340 and 445 °C observed for the pristine sample, thus suggesting changes in electrolyte composition by cycling in line with the macroscopic modifications displayed in Figure 3a and 3b. A residual mass of 43% is measured after complete degradation of the electrode support at 560 °C, accounting perhaps for possible crystalline Li_2S (melting point = 940 °C). The modifications of the cathode/polymer interface during cycling in the cell are further investigated by SEM in Figure 3e, which shows at the left-hand side a cross section image of a sample recovered after consecutive CV between 50

and 80 °C and on the right-hand side panel a graphic representation of the cathode/polymer-electrolyte stack with indication of the investigated area. In agreement with earlier reports,^[16,17,55] the SEM image of the composite clearly shows various layers, which are attributed to (i) the fibrous carbon-cloth electrode support (below the cyan mark in Figure 3e inset), (ii) the carbon coating of the electrode support along with the sulfur-carbon cathode film (gray layer between the cyan and the red marks in Figure 3e inset), and (iii) a portion of the PEGDME_CPE membrane (light gray layer between red marks in Figure 3e inset). Notably, our electron microscopy data suggest improved contact between the PEGDME_CPE and the sulfur-carbon electrode, which may favor the charge transfer at the interphase, as well contact regions in the electrolyte layer (colored by dark gray) which might be associated with the dissolution of lithium polysulfides during the electrochemical process. It is worth mentioning that PEGDME_CPE was not involved in the electrode formulation and the only polymeric species included in the cathode is poly(vinylidene fluoride) (PVDF), which acts as binding agent (see experimental section), although the addition of a polymer electrolyte to the cathode composition is a well-known technique to achieve the formation of an enhanced electrode/electrolyte interphase.^[43] Therefore, the formation of a suitable electrode/electrolyte interphase may be promoted by the relevant mobility of the PEGDME polymer chains at 50 °C, which is sufficient for allowing a proper cathode wetting and Li⁺ ions exchange. Furthermore, a contribution to the Li⁺ ions conductivity given by blending between PEGDME and PVDF cannot be excluded. On the other hand, the formation of a stable electrode/electrolyte assembly

is suggested by the SEM image in Figure 3e, which displays an adequate contact between the electrolyte and the cathode film.

The galvanostatic-cycling performance of the Li-S polymer battery at 50 °C is herein evaluated at the current rate of C/10 (1 C = 1675 mA g_s⁻¹). These testing conditions represent an optimal choice, which might match the typical requirements of the stationary storage market. We remark that the polymer configuration would ensure enhanced thermal stability, possibly allowing a safe use in large battery packs, whilst low current rate and moderately high temperature are well compatible with load-balancing applications in smart grids.^[21] Figure 4 shows the voltage profiles (panel a) and cycling behavior (panel b) of the above Li-S polymer cell, which steadily delivers a satisfactory capacity with high coulombic efficiency. In more detail, Figure 4a reveals the partial merging of the two characteristic plateaus at about 2.4 and 1.8 V upon the first discharge, accounting for the conversion of lithium and sulfur to lithium polysulfides (see CV in Figure 2a),^[63] as well as two definite charge plateaus at about 2.3 and 2.6 V. The sloping shape of the discharge plateau may suggest moderate Li⁺ diffusion hindering within the PEGDME_CPE as well as slow stabilization of the electrode/electrolyte interphase,^[64] which is gradually improved upon the subsequent cycles. Indeed, microstructural reorganizations due to polysulfide dissolution upon cycling^[16,17,55,56] favor a gradual change in cell response, leading to well-defined discharge plateaus at 2.4 and 1.9 V (Figure 4a). Furthermore, subsequent overlapping voltage curves characterized by moderate polarization between charge and discharge indicate a stable and efficient electrochemical process. In this regard, Figure 4b reveals a maximum capacity of 770 mAh g_s⁻¹, with a steady-state value ranging between 700 and

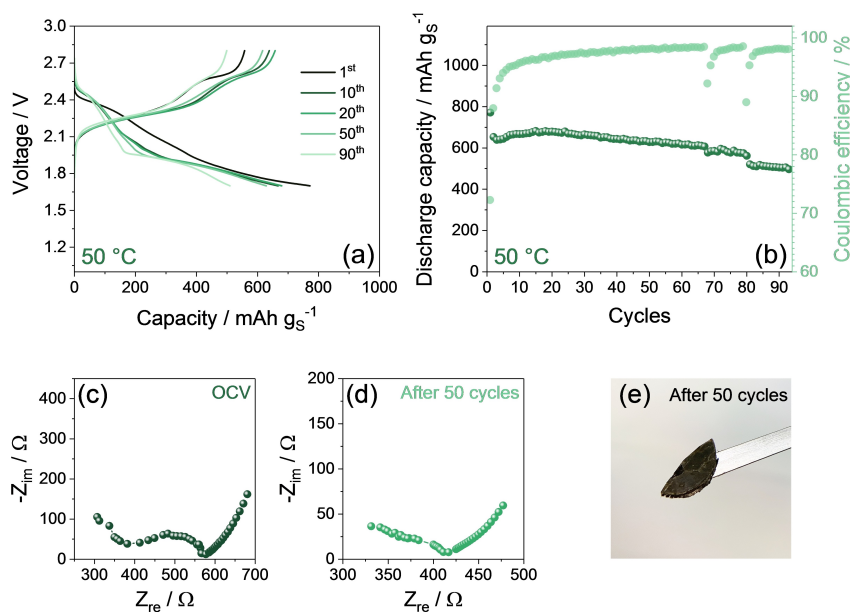


Figure 4. Electrochemical performance of the Li|PEGDME_CPE|S:SPC 70:30 w/w cell at 50 °C in terms of (a) voltage profiles and (b) cycling trend (discharge capacity in left-hand side y-axis and coulombic efficiency in right-hand side y-axis) at the constant current rate of C/10 (1 C = 1675 mA g_s⁻¹); voltage range: 1.7–2.8 V. (c, d) EIS measurements performed on a Li|PEGDME_CPE|S:SPC 70:30 w/w cell at 50 °C at various states, that is, (c) at the OCV condition and (d) after 50 discharge/charge cycles performed at C/10 (1 C = 1675 mA g_s⁻¹) between 1.7 and 2.8 V. EIS frequency range: 500 kHz–100 mHz; alternate voltage signal: 10 mV. (e) Photographic image of a PEGDME_CPE membrane on a S:SPC 70:30 w/w electrode recovered after the cycling test.

600 mAhg₅⁻¹, and a retention of 71% for over 90 cycles. Interestingly, the cell shows after the initial activation cycles a coulombic efficiency approaching 99%, except for few intermediate cycles particularly occurring at the final stages of the test, characterized by values decreasing down to about 90%, and raising again to the steady state (Figure 4b, light-green curve and right-side y-axis). This decrease in efficiency likely suggests the occurrence of micro-dendrites which are efficiently suppressed by the polymer electrolyte with the ongoing of the cycling to achieve the pristine efficiency value.^[42] This important aspect represent an additional bonus, in particular concerning the high safety content, of the PEGDME_CPE proposed herein for Li-S battery application. The stability of the electrode/electrolyte interphase is further demonstrated in Figure 4c and 4d, which reports the Nyquist plots at 50 °C of a Li-S cell employing the PEGDME_CPE at the OCV condition and after 50 cycles at C/10 (1 C = 1675 mA g₅⁻¹), respectively, while the related results of the NLLS analysis are displayed in Table 2. These Nyquist plots reveal a drop of the interphase resistance (R_i) upon cycling from about 180 Ω to 110 Ω (high-frequencies grain boundaries due to partial crystalline phase were not considered), denoting enhancements of the electrochemical activity at the electrode/electrolyte interphase by cycling in agreement with the EIS data reported in Figure 2 and Figure S3. In addition, the portion of cycled PEGDME_CPE/electrode sample recovered from the cell after 50 cycles is shown in Figure 4e, which reveals the formation of a blend between the electrolyte and the electrode evidencing suitable contact, while the dark red color of the cycled PEGDME_CPE membrane confirms the uniform dissolution of the lithium polysulfides during cell activity without any shuttle process, as also observed in Figure 3. These data clearly demonstrate the suitability of the Li-S system and display the stability of the electrode/electrolyte interphase upon cycling. Thus, considering an average capacity of 600 mAhg₅⁻¹ and an electrochemical process centered at 2.2 V, the Li-S polymer cell has a theoretical energy density of about 1300 Whkg⁻¹, which might lead to a suitable practical energy density and high efficiency for applications that require thermal stability.^[21] On the other hand, challenging operative conditions including high temperature may hinder the application of typical Li-S battery configurations based on volatile liquid electrolytes, as demonstrated in Figure S7 in the Supporting Information which shows a discharge/charge cycling test at the constant rate of C/10 (1 C = 1675 mA g₅⁻¹) performed at 50 °C on a Li-S battery employing the DOL:DME_LE. The voltage profiles displayed in Figure S7a reveal an irreversible discharge step at about 1.9 V likely ascribed to the reduction of LiNO₃

dissolved in the electrolyte solution promoted by the relatively high temperature, since this plateau it is usually observed around 1.6 V at room temperature.^[58] The excessive reduction of LiNO₃ may hinder electrode/electrolyte interphase, as suggested by the decay of capacity to around 900 mAhg₅⁻¹ (Figure S7b), which is a lower value with respect to the one delivered by the Li-S cell at 25 °C.^[55] Furthermore, both DOL and DME solvents suffer from marked volatility which may be promoted by the challenging temperature value, whilst the target performance of this liquid electrolyte is achieved at 25 °C.^[45-47,55] These data suggest the poor applicability of the DOL:DME solutions at high temperature, which, on the other hand, improves the performance of the PEGDME_CPE electrolyte.

3. Conclusions

To the best of our knowledge, we demonstrated for the first time that composite polymer electrolytes using PEGDME with MW of 2000 gmol⁻¹ as the solid solvent may be effectually applied in a Li-S battery operating at a temperature as low as 50 °C. The composite electrolyte membrane exhibited at 50 °C a Li⁺ transference number of 0.23 and an ionic conductivity of 1 × 10⁻⁴ Scm⁻¹, while the PEO-based benchmark electrolyte displayed similar t⁺ values (0.22) at 80 °C and considerably lower ionic conductivity (2 × 10⁻⁶ Scm⁻¹) at 50 °C.^[41] TGA evidenced a thermal stability extended up to 300 °C, suggesting suitable characteristics for applications requiring high safety level, such as the stationary energy-storage. Our data indicated that the polymer electrolyte forms a favorable interphase on both anode and cathode, which leads to a stable Li-S conversion process with low charge transfer resistance within the temperature range from 50 to 80 °C. In this interval, the polymer battery operated by electrochemical processes mainly centered at 2.4 and 2.0 V vs. Li⁺/Li during discharge and at 2.3 and 2.6 V vs. Li⁺/Li during charge, as revealed by CV, although above 60 °C we observed enhanced conversion kinetics, leading to better overlapping of the potential profiles and more intense current signals. This promising cell response was attributed to the suitably low resistance of both electrode/electrolyte interphase (between 83 and 12 Ω) and electrolyte (between 304 and 55 Ω), which was measured by EIS in the 50–80 °C range. Furthermore, increase in temperature gave rise to a third discharge step at 2.3 V vs. Li⁺/Li along with a gradual shift of the charge peaks up to formation of a broad double-signal similar to that observed in Li-S cells using a conventional liquid electrolyte. Indeed, the polymer system revealed a profile change from *solid-like* to *liquid-like* Li-S battery upon increasing the temperature from 50 °C to 80 °C. Accordingly, this work has provided evidence of lithium polysulfide dissolution into the electrolyte upon cell operation, which influenced the thermal and morphological characteristics of the cathode/electrolyte-membrane array. The Li-S polymer battery operated at 50 °C with a working voltage of 2.2 V, delivering a capacity above 600 mAhg₅⁻¹ at C/10 (1 C = 1675 mA g₅⁻¹), with a retention of 71% for more than 90 discharge/charge cycles and a maximum

Table 2. S:SPC 70:30 w/w/PEGDME_CPE interphase resistance (R_i) obtained by nonlinear least squares (NLLS) analysis of the EIS data via the Boukamp software.^[66,67] The EIS data have been collected at 50 °C during a galvanostatic cycling measurement on the Li|PEGDME_CPE|S:SPC 70:30 w/w cell. See the Experimental section of the manuscript for sample acronyms and Figure 4 (c, d) for relevant Nyquist plots.

Cell condition	Circuit	R _i [Ω]	χ ²
OCV	R _e (R _i Q _i)Q _w	179 ± 10	8 × 10 ⁻⁵
After 50 cycles	R _e (R _i Q _i)Q _w	108 ± 17	3 × 10 ⁻⁵

coulombic efficiency of 98%. It is worth mentioning that the reversibility of the cell may be further improved by carefully tuning the electrolyte composition in terms of amounts of sacrificial additive (e.g., LiNO₃) and ceramic (e.g., SiO₂), in order to enhance the SEI layer on the electrodes surface. Therefore, our study suggests a new pathway to achieve safe lithium-metal cell exploiting the high-energy Li–S conversion process.

Experimental

Achievement of the Composite Polymer Electrolyte

The composite polymer electrolyte (CPE) was prepared by mixing polyethylene glycol dimethyl ether (PEGDME2000, CH₃O-(C₂H₄O)_n-CH₃, average MW of 2000 g mol⁻¹, Sigma-Aldrich), lithium bis(trifluoromethanesulfonyl)imide (LiTFSI, 99.95% trace metals basis, Sigma-Aldrich), lithium nitrate (LiNO₃, 99.99% trace metals basis, Sigma-Aldrich), and fumed silica (SiO₂, average particle size: 0.007 μm, Sigma-Aldrich). Before use, LiTFSI and LiNO₃ were dried under vacuum for two days at 110 °C. Either salts were added to the PEGDME2000 in the 1 mol kg⁻¹ concentration as referred to the mass of the latter, and 10 wt.% SiO₂ (as referred to the mass of PEGDME2000-lithium salts mixture) was incorporated in the CPE. The solid electrolyte membrane was obtained by forming a dense, semi-liquid slurry of the above components with acetonitrile (ACN, Sigma-Aldrich), which was subsequently removed upon several drying steps at various temperatures as reported in a previous work.^[42] This CPE is herein indicated as PEGDME_CPE.

Preparation of a Control Liquid Electrolyte

A control liquid electrolyte (LE) was prepared by dissolving LiTFSI (1 mol kg_{solvent}⁻¹) and LiNO₃ (1 mol kg_{solvent}⁻¹) in a solution of 1,3-dioxolane (DOL, anhydrous, containing ca. 75 ppm of butylated hydroxytoluene, i.e., BHT, as inhibitor, 99.8%, Sigma-Aldrich) and 1,2-dimethoxyethane (DME, anhydrous, inhibitor-free, 99.5%, Sigma-Aldrich) in the 1:1 weight ratio. Prior to use, both DOL and DME were dried by molecular sieves (3 Å, rod, size 1/16 in., Honeywell Fluka) until a water content below 10 ppm was obtained as measured by 899 Karl Fischer Coulometer, Metrohm, whilst LiTFSI and LiNO₃ were dried under vacuum for two days at 110 °C as above mentioned. This LE is herein indicated as DOL:DME_LE.

Preparation of the Sulfur Electrode

The sulfur-carbon composite was prepared as described previously,^[55] by mixing elemental sulfur (S, ≥99.5%, Riedel-Haën) and conductive carbon black (Super P, Timcal, SPC) by the weight ratio of 70:30 under magnetic stirring in a silicone oil bath at about 125 °C. The resulting composite was subsequently cooled down to room temperature and ground in an agate mortar to obtain a fine powder. This composite is herein referred as S:SPC 70:30 w/w. Sulfur electrode disks were obtained through doctor blade casting (MTI Corp.) of a slurry formed by 80 wt% sulfur-carbon composite (i.e., S:SPC 70:30 w/w), 10 wt% conductive carbon black (Super P, Timcal, SPC), and 10 wt% poly(vinylidene fluoride) binder (Solef® 6020 PVDF) homogeneously dispersed in *N*-methyl-2-pyrrolidone (NMP, Sigma-Aldrich). The slurry was cast on a porous carbon-cloth foil (GDL ELAT 1400, MTI Corp.), which was then heated on a hot plate at 50 °C for about 3 h under a fume hood. Afterwards, electrode disks with diameter of 14 mm and 10 mm were cut out from the coated carbon-cloth and dried overnight at 35 °C under vacuum before being transferred in argon-

filled glovebox (MBraun, H₂O and O₂ content below 1 ppm). The obtained sulfur loading on the electrodes was about 1 mg cm⁻².

Cell Assembly and Electrochemical Tests

CR2032 coin-type cells (MTI Corp.) were assembled in an argon-filled glovebox (MBraun, H₂O and O₂ content below 1 ppm) and studied by using various electrochemical techniques. The electrolyte lithium transference number (*t*⁺) was evaluated according to the Bruce-Vincent-Evans method,^[65] by applying to a symmetrical Li|Li cell a voltage of 30 mV for 90 minutes (chronoamperometry measurement) and collecting impedance spectra of this cell before and after polarization. The alternate voltage bias of these EIS measurements had an amplitude of 10 mV, and the frequency investigated ranged from 500 kHz to 100 mHz. The *t*⁺ value was calculated using equation (1):^[65]

$$t^+ = \frac{i_{ss}}{i_0} \frac{\Delta V - i_0 R_0}{\Delta V - i_{ss} R_{ss}} \quad (1)$$

where Δ*V* is the chronoamperometry voltage (i.e., 30 mV), *i*₀ is the initial current during polarization, *i*_{ss} is the final current, and *R*₀ and *R*_{ss} are the electrode/electrolyte interphase resistance determined by EIS before and after the 90-minute polarization, respectively.

The ionic conductivity of the electrolytes was extracted from EIS data, which were collected by applying to a symmetrical cell with stainless steel (SS) electrodes an alternate voltage signal amplitude of 10 mV within the 500 kHz–100 Hz frequency range.

Li|PEGDME_CPE|S:SPC 70:30 w/w cells were assembled by stacking a lithium disk with a diameter of 14 mm, with PEGDME_CPE membrane and S:SPC 70:30 w/w electrode having diameters of 10 mm housed into 4 polymeric O-rings (CS Hyde, 23-5FEP-2-50) with internal diameter of 10 mm, and thickness of 127 μm each. Prior to the tests, all the Li|PEGDME_CPE|S:SPC 70:30 w/w cells were exposed to 4 heating-cooling cycles between 25 and 70 °C to decrease the crystallinity and enhance the ionic conductivity of the PEGDME_CPE; each cycle had a duration of 24 h (i.e., 12 h for each heating and cooling step).^[42] Li|DOL:DME_LE|S:SPC 70:30 w/w control cells were assembled by employing a 14-mm diameter sulfur-carbon electrode separated from the lithium anode by a 16-mm diameter Celgard 2400 foil soaked with 25 μL of electrolyte solution for CV tests and 15 μL mg_s⁻¹ for galvanostatic cycling, as previously reported.^[55] CV measurements were carried out on a Li|PEGDME_CPE|S:SPC 70:30 w/w cell at 50, 60, 70, and 80 °C, as well as on a Li|DOL:DME_LE|S:SPC 70:30 w/w control cell at room temperature, by employing a scan rate of 0.1 mV s⁻¹ in the 1.8–2.8 V vs. Li⁺/Li potential range. EIS measurements were performed on these cells at the OCV condition as well as upon the voltammetry cycles at the above-mentioned temperature conditions, by applying an alternate voltage signal with amplitude of 10 mV within the 500 kHz–100 mHz frequency range. The impedance spectra were analyzed with the Boukamp software using the non-linear least squares (NLLS) method (the χ² was in the order of 10⁻⁴ or lower).^[66,67] The impedance response of the cell was modelled by using equivalent circuits which incorporate the high-frequency electrolyte resistance (*R*_e), high-to-middle frequency resistive and constant phase elements (*R*_i*Q*_i) arranged in parallel and ascribed to the electrode/electrolyte interphase, as well as low frequency elements accounting for the Warburg-type, Li⁺ diffusion (*R*_w and *Q*_w).^[66,67] Galvanostatic cycling tests were performed on Li|PEGDME_CPE|S:SPC 70:30 w/w and Li|DOL:DME_LE|S:SPC 70:30 w/w cells at the constant current rate of C/10 (1 C = 1675 mA g_s⁻¹) in the 1.7–2.8 V voltage range for the former and between 1.9 and 2.8 V for the latter at 50 °C through a MACCOR Series 4000 battery

test system. EIS data were collected on a Li|PEGDME_CPE|S:SPC 70:30 w/w cell at the OCV condition and after 50 discharge/charge galvanostatic cycles. All CV, EIS and chronoamperometry data were collected using a VersaSTAT MC Princeton Applied Research (PAR, AMETEK) instrument.

SEM and Thermogravimetric Analyses of the Electrode/Electrolyte Assembly

SEM images of a PEGDME_CPE membrane on a S:SPC 70:30 w/w electrode recovered after the CV measurement in Li cell were collected using a Zeiss EVO 40 microscope with a LaB₆ thermionic source. TGA was carried out under a N₂ atmosphere and employing a heating rate of 5°C min⁻¹ in the 25–800°C temperature range, through a Mettler-Toledo TGA 2 instrument. Several samples were investigated by TGA: (i) PEGDME2000 powder, (ii) PEGDME_CPE membrane and (iii, iv) PEGDME_CPE on a S:SPC 70:30 w/w electrode in pristine condition and after CV. The samples were transferred quickly from the glovebox to the SEM and TGA chambers for measurements, in order to avoid excessive exposure to the atmosphere and limit moisture absorption.

Acknowledgements

This work has received funding from the European Union's Horizon 2020 research and innovation programme Graphene Flagship under grant agreement No 881603, and the grant "Fondo per l'Incentivazione alla Ricerca (FIR) 2020", University of Ferrara. The authors acknowledge the project "Accordo di Collaborazione Quadro 2015" between University of Ferrara (Department of Chemical, Pharmaceutical and Agricultural Sciences) and Sapienza University of Rome (Department of Chemistry). Open Access Funding provided by Università degli Studi di Ferrara within the CRUI-CARE Agreement.

Conflict of Interest

The authors declare no conflict of interest.

Keywords: poly(ethylene glycol) dimethyl ether · solid PEGDME · composite polymer electrolyte · Li–S battery · lithium polymer battery.

- [1] L. Carbone, S. G. Greenbaum, J. Hassoun, *Sustain. Energy Fuels* **2017**, *1*, 228.
- [2] K. Cai, M.-K. Song, E. J. Cairns, Y. Zhang, *Nano Lett.* **2012**, *12*, 6474.
- [3] Z. Li, Y. Huang, L. Yuan, Z. Hao, Y. Huang, *Carbon* **2015**, *92*, 41.
- [4] B. Scrosati, J. Hassoun, Y.-K. Sun, *Energy Environ. Sci.* **2011**, *4*, 3287.
- [5] P. G. Bruce, S. A. Freunberger, L. J. Hardwick, J.-M. Tarascon, *Nat. Mater.* **2012**, *11*, 19.
- [6] R. Fang, S. Zhao, Z. Sun, D.-W. Wang, R. Amal, S. Wang, H.-M. Cheng, F. Li, *Energy Storage Mater.* **2018**, *10*, 56.
- [7] J. B. Robinson, K. Xi, R. V. Kumar, A. C. Ferrari, H. Au, M.-M. Titirici, A. Parra-Puerto, A. Kucernak, S. D. S. Fitch, N. Garcia-Araez, Z. L. Brown, M. Pasta, L. Furness, A. J. Kibler, D. A. Walsh, L. R. Johnson, C. Holc, G. N. Newton, N. R. Champness, F. Markoulidis, C. Crean, R. C. T. Slade, E. I. Andritsos, Q. Cai, S. Babar, T. Zhang, C. Lekakou, N. Kulkarni, A. J. E. Rettie, R. Jarvis, M. Cornish, M. Marinescu, G. Offer, Z. Li, L. Bird, C. P. Grey, M. Chhowalla, D. Di Lecce, R. E. Owen, T. S. Miller, D. J. L. Brett, S. Liatard, D. Ainsworth, P. R. Shearing, *J. Phys. Energy* **2021**, *3*, 031501.
- [8] R. Fang, G. Li, S. Zhao, L. Yin, K. Du, P. Hou, S. Wang, H.-M. Cheng, C. Liu, F. Li, *Nano Energy* **2017**, *42*, 205.
- [9] J.-Y. Hwang, S. Shin, C. S. Yoon, Y.-K. Sun, *ACS Energy Lett.* **2019**, *4*, 2787.
- [10] L. Carbone, T. Coneglian, M. Gobet, S. Munoz, M. Devany, S. Greenbaum, J. Hassoun, *J. Power Sources* **2018**, *377*, 26.
- [11] Y. Cui, X. Wu, J. Wu, J. Zeng, A. P. Baker, F. Lu, X. Liang, J. Ouyang, J. Huang, X. Liu, Z. Li, X. Zhang, *Energy Storage Mater.* **2017**, *9*, 1.
- [12] T. Wang, Y. Yang, L. Fan, L. Wang, R. Ma, Q. Zhang, J. Zhao, J. Ge, X. Lu, X. Yu, H. Yang, B. Lu, *ACS Appl. Mater. Interfaces* **2018**, *1*, 7076.
- [13] K. Xiao, J. Wang, Z. Chen, Y. Qian, Z. Liu, L. Zhang, X. Chen, J. Liu, X. Fan, Z. X. Shen, *Small* **2019**, *15*, 1901454.
- [14] A. Benítez, V. Marangon, C. Hernández-Rentero, Á. Caballero, J. Morales, J. Hassoun, *Mater. Chem. Phys.* **2020**, *255*, 123484.
- [15] Y. Jiang, H. Zhao, L. Yue, J. Liang, T. Li, Q. Liu, Y. Luo, X. Kong, S. Lu, X. Shi, K. Zhou, X. Sun, *Electrochem. Commun.* **2021**, *122*, 106881.
- [16] V. Marangon, D. Di Lecce, F. Orsatti, D. J. L. Brett, P. R. Shearing, J. Hassoun, *Sustain. Energy Fuels* **2020**, *4*, 2907.
- [17] V. Marangon, D. Di Lecce, D. J. L. Brett, P. R. Shearing, J. Hassoun, *J. Energy Chem.* **2022**, *64*, 116.
- [18] S. S. Zhang, *J. Power Sources* **2016**, *322*, 99.
- [19] W. Li, H. Yao, K. Yan, G. Zheng, Z. Liang, Y.-M. Chiang, Y. Cui, *Nat. Commun.* **2015**, *6*, 7436.
- [20] H. Zhang, G. G. Eshetu, X. Judez, C. Li, L. M. Rodríguez-Martínez, M. Armand, *Angew. Chem. Int. Ed.* **2018**, *57*, 15002.
- [21] A. Varzi, K. Thanner, R. Scipioni, D. Di Lecce, J. Hassoun, S. Dörfler, H. Altheus, S. Kaskel, C. Prehal, S. A. Freunberger, *J. Power Sources* **2020**, *480*, 228803.
- [22] J. Gao, M. A. Lowe, Y. Kiya, H. D. Abruña, *J. Phys. Chem. C* **2011**, *115*, 25132.
- [23] S. Zhang, K. Ueno, K. Dokko, M. Watanabe, *Adv. Energy Mater.* **2015**, *5*, 1.
- [24] S. Kim, Y. Jung, H. S. Lim, *Electrochim. Acta* **2004**, *50*, 889.
- [25] L. Carbone, M. Gobet, J. Peng, M. Devany, B. Scrosati, S. Greenbaum, J. Hassoun, *ACS Appl. Mater. Interfaces* **2015**, *7*, 13859.
- [26] T. Seita, Y. Matsumae, J. Liu, R. Tatara, K. Ueno, K. Dokko, M. Watanabe, *ACS Energy Lett.* **2020**, *5*, 1.
- [27] D. Di Lecce, L. Minnetti, D. Polidoro, V. Marangon, J. Hassoun, *Ionics* **2019**, *25*, 3129.
- [28] Z. Xue, D. He, X. Xie, *J. Mater. Chem. A* **2015**, *3*, 19218.
- [29] F. Croce, G. B. Appetecchi, L. Persi, B. Scrosati, *Nature* **1998**, *394*, 456.
- [30] B. W. Zewde, S. Admassie, J. Zimmermann, C. S. Isfort, B. Scrosati, J. Hassoun, *ChemSusChem* **2013**, *6*, 1400.
- [31] W. Lyu, G. He, T. Liu, *ChemistryOpen* **2020**, *9*, 713.
- [32] D. Lin, W. Liu, Y. Liu, H. R. Lee, P. C. Hsu, K. Liu, Y. Cui, *Nano Lett.* **2016**, *16*, 459.
- [33] R. Lei, Y. Yang, C. Yu, Y. Xu, Y. Li, J. Li, *Sustain. Energy Fuels* **2021**, *5*, 1538.
- [34] L. Zhong, S. Wang, M. Xiao, W. Liu, D. Han, Z. Li, J. Qin, Y. Li, S. Zhang, S. Huang, Y. Meng, *Energy Storage Mater.* **2021**, *41*, 563.
- [35] A. Santiago, J. Castillo, I. Garbayo, A. Saenz de Buruaga, J. A. Coca Clemente, L. Qiao, R. Cid Barreno, M. Martínez-Ibañez, M. Armand, H. Zhang, C. Li, *ACS Appl. Mater. Interfaces* **2021**, *4*, 4459.
- [36] X. Zhang, T. Zhang, Y. Shao, H. Cao, Z. Liu, S. Wang, X. Zhang, *ACS Sustainable Chem. Eng.* **2021**, *9*, 5396.
- [37] I. Gracia, H. Ben Youcef, X. Judez, U. Oteo, H. Zhang, C. Li, L. M. Rodríguez-Martínez, M. Armand, *J. Power Sources* **2018**, *390*, 148.
- [38] X. Judez, H. Zhang, C. Li, G. G. Eshetu, Y. Zhang, J. A. González-Marcos, M. Armand, L. M. Rodríguez-Martínez, *J. Phys. Chem. Lett.* **2017**, *8*, 3473.
- [39] L. Carbone, J. Hassoun, *Ionics* **2016**, *22*, 2341.
- [40] X.-L. Wang, A. Mei, X.-L. Li, Y.-H. Lin, C.-W. Nan, *J. Power Sources* **2007**, *171*, 913.
- [41] G. Derrien, J. Hassoun, S. Sacchetti, S. Panero, *Solid State Ionics* **2009**, *180*, 1267.
- [42] V. Marangon, Y. Tominaga, J. Hassoun, *J. Power Sources* **2020**, *449*, 227508.
- [43] D. Marmorstein, T. H. Yu, K. a. Striebel, F. R. McLarnon, J. Hou, E. J. Cairns, *J. Power Sources* **2000**, *89*, 219.
- [44] J. Hassoun, B. Scrosati, *Angew. Chem. Int. Ed.* **2010**, *49*, 2371.
- [45] J. Chang, J. Shang, Y. Sun, L. K. Ono, D. Wang, Z. Ma, Q. Huang, D. Chen, G. Liu, Y. Cui, Y. Qi, Z. Zheng, *Nat. Commun.* **2018**, *9*, 4480.
- [46] Y. An, C. Luo, D. Yao, S. Wen, P. Zheng, S. Chi, Y. Yang, J. Chang, Y. Deng, C. Wang, *Nano-Micro Lett.* **2021**, *13*, 84.
- [47] M. Rana, Q. He, B. Luo, T. Lin, L. Ran, M. Li, I. Gentle, R. Knibbe, *ACS Cent. Sci.* **2019**, *5*, 1946.

- [48] S. Wei, S. Inoue, D. Di Lecce, Z. Li, Y. Tominaga, J. Hassoun, *ChemElectroChem* **2020**, *7*, 2344.
- [49] J. Popovic, G. Hasegawa, I. Moudrakovski, J. Maier, *J. Mater. Chem. A* **2016**, *4*, 7135.
- [50] D. Di Lecce, V. Sharova, S. Jeong, A. Moretti, S. Passerini, *Solid State Ionics* **2018**, *316*, 66.
- [51] J. Xie, R. G. Duan, Y. Han, J. B. Kerr, in *Solid State Ionics*, **2004**, pp. 755–758.
- [52] R. Frech, W. Huang, *Macromolecules* **1995**, *28*, 1246.
- [53] V. Marangon, C. Hernandez-Rentero, S. Levchenko, G. Bianchini, D. Spagnolo, A. Caballero, J. Morales, J. Hassoun, S. Cathode, *ACS Appl. Mater. Interfaces* **2020**, *3*, 12263.
- [54] A. Benítez, A. Caballero, J. Morales, J. Hassoun, E. Rodríguez-Castellón, J. Canales-Vázquez, *Nano Res.* **2019**, *12*, 759.
- [55] D. Di Lecce, V. Marangon, W. Du, D. J. L. Brett, P. R. Shearing, J. Hassoun, *J. Power Sources* **2020**, *472*, 228424.
- [56] C. Tan, T. M. M. Heenan, R. F. Ziesche, S. R. Daemi, J. Hack, M. Maier, S. Marathe, C. Rau, D. J. L. Brett, P. R. Shearing, *ACS Appl. Mater. Interfaces* **2018**, *1*, 5090.
- [57] Y. Chen, S. Lu, J. Zhou, W. Qin, X. Wu, *Adv. Funct. Mater.* **2017**, *27*, 1700987.
- [58] D. Di Lecce, V. Marangon, A. Benítez, Á. Caballero, J. Morales, E. Rodríguez-Castellón, J. Hassoun, *J. Power Sources* **2019**, *412*, 575.
- [59] G. B. Appetecchi, F. Croce, J. Hassoun, B. Scrosati, M. Salomon, F. Cassel, *J. Power Sources* **2003**, *114*, 105.
- [60] X. Judez, H. Zhang, C. Li, J. A. González-Marcos, Z. Zhou, M. Armand, L. M. Rodríguez-Martínez, *J. Phys. Chem. Lett.* **2017**, *8*, 1956.
- [61] J. Guo, X. Du, X. Zhang, F. Zhang, J. Liu, *Adv. Mater.* **2017**, *29*, 1700273.
- [62] J. Yao, T. Mei, Z. Cui, Z. Yu, K. Xu, X. Wang, *Chem. Eng. J.* **2017**, *330*, 644.
- [63] F. Luna-Lama, C. Hernández-Rentero, Á. Caballero, J. Morales, *Electrochim. Acta* **2018**, *292*, 522.
- [64] G. B. Appetecchi, J. Hassoun, B. Scrosati, F. Croce, F. Cassel, M. Salomon, *J. Power Sources* **2003**, *124*, 246.
- [65] J. Evans, C. a. Vincent, P. G. Bruce, *Polymer* **1987**, *28*, 2324.
- [66] B. A. Boukamp, *Solid State Ionics* **1986**, *20*, 31.
- [67] B. A. Boukamp, *Solid State Ionics* **1986**, *18–19*, 136.

Manuscript received: September 17, 2021
Revised manuscript received: September 24, 2021
Accepted manuscript online: September 27, 2021